COMMUNICATION

Check for updates

Lead-free, stable, high-efficiency (52%) blue luminescent $FA_3Bi_2Br_9$ perovskite quantum dots†

Yalong Shen,[a] Jun Yin, [iD][b] Bo Cai,[a] Ziming Wang,[a] Yuhang Dong,[a] Xiaobao Xu[a] and Haibo Zeng [iD] *[a]

Lead halide perovskites are promising candidates as next-generation emitting materials for lighting and displays due to their superior properties. However, the toxicity of lead content severely limits their practical applications. Although lead-free Sn-based and Bi-based perovskites ($Cs_3Bi_2Br_9$, $MA_3Bi_2Br_9$) are reported, they all suffer from low photoluminescence quantum yield (PLQY). Here, we report the synthesis of lead-free $FA_3Bi_2Br_9$ perovskite quantum dots (QDs) and their optical characterization. Through a facile ligand-assisted solution process, the as-synthesized $FA_3Bi_2Br_9$ QDs exhibit a bright blue emission at 437 nm with a high PLQY of 52%. As to the origins, the observed high exciton binding energy (274.6 meV), direct band-gap nature and low defect density are proposed to guarantee the exciton generation and efficient radiative recombination. Besides, the $FA_3Bi_2Br_9$ QDs show a good air stability and ethanol stability. A lead-free perovskite blue light-emitting diodes (LED) was success-fully fabricated by combining $FA_3Bi_2Br_9$ QDs/PS composites with a UV light chip. Our results highlight the potential of lead-free perovskites for applications in light-emitting devices.

Introduction

Over the past few decades, semiconductor quantum dot (QD) materials have been successfully developed due to their unique photonic and electronic properties.[1–4] In particular, lead (Pb) halide perovskite QDs exhibit ultrahigh photoluminescence quantum yield (PLQY, 70–100%), wide color gamut (~150% NTSC) and flexible bandgap tunability, enabling them to be ideal candidates as a new generation of light-emitting diodes (LEDs) for lighting and displays.[5–11] The LEDs based on perovskite QDs show excellent performance and most of them were

New concepts

For the three-primary-color displays of perovskite nanocrystals (NCs), blue emission always suffers from low photoluminescence quantum yield (PLQY), lagging behind those of green and red ones severely. Simultaneously, replacement of lead with low toxicity elements in perovskites is preferred toward potential applications. In this paper, an exceptionally simple solution process is developed to synthesize a lead-free Bi-based $FA_3Bi_2Br_9$ perovskite quantum dots (QDs) with ligand-assistance. The as-prepared $FA_3Bi_2Br_9$ QDs exhibit a high PLQY over 50% in the blue-emitting region, and these quantum-confined QDs were measured to possess a high exciton binding energy, which ensures the generation of excitons and their high-rate recombination. The ligand passivation of the $FA_3Bi_2Br_9$ QDs helps suppress the surface defects and thus enhances the PLQY. Besides, the $FA_3Bi_2Br_9$ QDs were demonstrated to have a direct bandgap and a backlit LED was constructed based on them.

assembled with low-cost solution processes. Despite the above outstanding properties, the intrinsic toxicity of Pb-based perovskites greatly hinders their practical applications.[12–14] Therefore, developing non-toxic lead-free perovskites that retain compar-able photoelectric properties with lead halide perovskites has become a practically important task.

In literature reports, several non-toxic metals have been proposed to replace Pb, such as tin (Sn), manganese (Mn), and bismuth (Bi).[15–17] Replacing Pb^{2+} with divalent Sn^{2+} was first considered, and the achieved Sn-based perovskites can well maintain the three-dimensional (3D) perovskite structure. Unfortunately, the $ASnX_3$ (A = Cs, MA, FA, X = Cl, Br, and I) perovskites are very sensitive to the ambient atmosphere (oxygen, moisture, and light) since Sn^{2+} can be easily oxidized to Sn^{4+}. To our best knowledge, the highest reported PLQY of $CsSnX_3$ is below 1%.[18] The vacancy-ordered double perovskites Cs_2SnX_6 possess a good stability, but still suffer from a low PLQY.[19–22] Another divalent cation Mn^{2+} can be doped into the lead-based perovskites but without full substitution of Pb^{2+} cations, and could only achieve a half PLQY value as compared to their lead-containing analogues.[23,24]

Bismuth (Bi) and Pb are adjacent in the same row of the periodic table, and Bi is less toxic than Pb. Bi ($6s^2 6p^3$) holds the

[a] MIIT Key Laboratory of Advanced Display Materials and Devices, Institute of Optoelectronics & Nanomaterials, College of Materials Science and Engineering, Nanjing University of Science and Technology, Nanjing, Jiangsu, 210094, China. E-mail: zeng.haibo@njust.edu.cn

[b] Division of Physical Sciences and Engineering, King Abdullah University of Science and Technology, Thuwal 23955-6900, Kingdom of Saudi Arabia

† Electronic supplementary information (ESI) available. See DOI: 10.1039/c9nh00685k

same lone-pair $6s^2$ state as Pb ($6s^26p^2$), exhibiting close energy levels and similar electronic properties with Pb. Different from the stoichiometry in Pb-based perovskites, the Bi-based perovskites show an $A_3Bi_2X_9$ configuration, and in order to keep charge balance, Bi^{3+} produces a layered form of the vacancy-ordered perovskite unit cell with only two-thirds of the octahedral positions fully occupied, reducing the crystal dimensionality from 3D to two-dimensions (2D).[16] More recently, Tang and coworkers reported the organic–inorganic hybrid Bi-based perovskite $MA_3Bi_2Br_9$ QDs with 2D electronic structure and achieved the PLQY of 12% in the blue region (423 nm), and the $MA_3Bi_2Br_9$ QDs exhibited a good ethanol stability.[25] Leng et al. prepared more stable all-inorganic Bi-based $Cs_3Bi_2Br_9$ nanocrystals, achieving a blue emission light at 410 nm with PLQY reaching 19.4%.[26] However, the PLQYs of Bi-based perovskites are still far behind Pb-based counterparts.

Herein, we report the synthesis and optical characterization of Pb-free $FA_3Bi_2X_9$ ($FA^+ = NH_2HCNH_2^+$) perovskite QDs. Colloidal $FA_3Bi_2Br_9$ QDs were prepared via a convenient solution synthesis process with ligand-assisted. The as-synthesized $FA_3Bi_2Br_9$ QDs exhibit a blue emission peak located at 437 nm with a high PLQY up to 52%. This high PLQY value is among the highest ones for Pb-free perovskites in the blue-emitting region, and comparable to those of Pb-based perovskites. Two points account for this high PLQY value. First and foremost, the $FA_3Bi_2Br_9$ QDs show an extremely low defect density due to the ligand surface passivation, which suppresses the non-radiative recombination channels. Second, the big exciton binding energy (E_b) of the QDs, enables efficient radiative recombination of excitons, which, in principle, boosts the PLQY. Thanks to the Br-rich component and ligand-passivation effect, the typical $FA_3Bi_2Br_9$ QDs are found to possess a good air-stability and superior ethanol stability. Furthermore, we combined the $FA_3Bi_2Br_9$ QDs with commercial UV light chips to construct a LED, and demonstrated their promising applications in blue light emission.

Results and discussion

The $FA_3Bi_2Br_9$ QDs were synthesized by using a facile solution process at room temperature (see the experimental details in the ESI†), and the solid $FA_3Bi_2Br_9$ powder was also obtained by rotary evaporation for characterization analysis (Fig. S1, ESI†). A mixture of DMF and DMSO were used as the solvent to dissolve FABr and $BiBr_3$ to form the precursor solution, the surface ligand oleic acids (OA) and oleylamine (OAm) was dissolved in toluene to control the crystallization and passivation of the QD surface. During the synthesis process, by adjusting the precursor concentration and the amount of ligand, the highest PL intensity was achieved by the sample, and the results are shown in Fig. S2 (ESI†). The as-prepared $FA_3Bi_2Br_9$ QD solution exhibits bright blue color under UV-light irradiation, and the corresponding PLQY was measured to be as high as 52%, which is not the highest but better than most other Pb-free perovskite QDs (Table S1, ESI†).[27]

X-ray diffraction (XRD) measurements of the $FA_3Bi_2Br_9$ powder sample were conducted to study the crystal structural information, and the results are presented in Fig. 1a ($a = b = 7.96$ Å, $c = 9.78$ Å, $\alpha = \beta = 90°$, $\gamma = 120°$), confirming that the perovskite is crystalline with the hexagonal structure and holds the trigonal $P3m1$ space group (No. 164), which is consistent with our calculated patterns and the previous reports on similar compounds.[28] As illustrated in Fig. 1b, the crystal structure of $FA_3Bi_2Br_9$ perovskite shows that one FA^+ group is surrounded by six metal halide octahedral layers, the $BiBr_6$ octahedra is fused into $Bi_2Br_9^{3-}$ dimers through sharing their triangular faces, and it is derived from the 3D ABX_3 perovskite by moving every third Bi layer along (111) to achieve correct charge balance, forming a quasi-2D structure (Fig. 1c). The characterization was taken by TEM and high-resolution TEM (HRTEM) measurements, as shown in Fig. 1d. According to the typical TEM images, the as-synthesized $FA_3Bi_2Br_9$ QDs are polydisperse with a partially quasi-spherical shape, which exhibits an average size of 4.9 ± 0.8 nm (Fig. 1e). The HRTEM image of $FA_3Bi_2Br_9$ QDs reveals a high crystallinity with the typical interplanar distance of 0.34 nm, matching well with that of the (003) plane in an $FA_3Bi_2Br_9$ structure ($d_{(003)} = 0.341$ nm). The selected-area electron-diffraction (SAED) pattern of an individual QD in Fig. 1f confirms the highly crystalline nature of the $FA_3Bi_2Br_9$ QDs with a hexagonal diffraction pattern, again in agreement with the XRD patterns.

We further carried out X-ray photoelectron spectroscopy (XPS) measurements to evaluate the surface chemistry of the $FA_3Bi_2Br_9$ perovskite. As given in Fig. S3 (ESI†), the presence of Bi and Br is clearly presented in survey XPS spectra, and the Br/Bi ratio of the QD sample is 4.9, which is higher than the ideal atomic ratio (4.5) according to the chemical formula. The achieved Br-rich $FA_3Bi_2Br_9$ QDs may increase the air-stability of the perovskite under ambient conditions. The high-resolution XPS spectra of N (1s), Bi (4f), and Br (3d) are shown in Fig. 1g–i. We find that the two XPS peaks of Bi-4f at binding energy of 158.2 and 163.7 eV, respectively, are attributed to the $4f_{7/2}$ and $4f_{5/2}$ bonding of Bi^{3+}. The Br-3d peaks can be fitted into two peaks at binding energies of 66.9 and 68.0 eV, which correspond to the $3d_{5/2}$ and $3d_{3/2}$ bonding of Br^-, respectively. Two peaks at 398.1 and 400.6 eV can be found in the N 1s XPS spectrum, indicating that there are two existing chemical states of N element, one was attributed to FA^+ and the other to the surface OAm^+ of $FA_3Bi_2Br_9$ QDs.

Fig. 2a shows the absorption and photoluminescence (PL) spectra of the colloidal $FA_3Bi_2Br_9$ QDs solution (the insets show the photographs of the QD solution under light and UV-irradiation). The $FA_3Bi_2Br_9$ QD solution shows a clear pale-yellow color under sunlight, which is a good indication of the $FA_3Bi_2Br_9$ QD nucleation without any aggregation. While under UV-irradiation, a bright blue color can be clearly observed, implying outstanding PL properties of the $FA_3Bi_2Br_9$ QDs. The absorption spectra of $FA_3Bi_2Br_9$ QDs show a pronounced band edge exciton peak at 404 nm, and PL spectra centered at 437 nm with a broad full width at half maxima (FWHM) of 65 nm. The Stokes shift of the sample was determined to be 231 meV, which indicates almost no overlap between absorption and PL spectra.[29] Such large Stokes shift renders the QDs a weak self-absorption, making them appropriate for usage as a phosphor
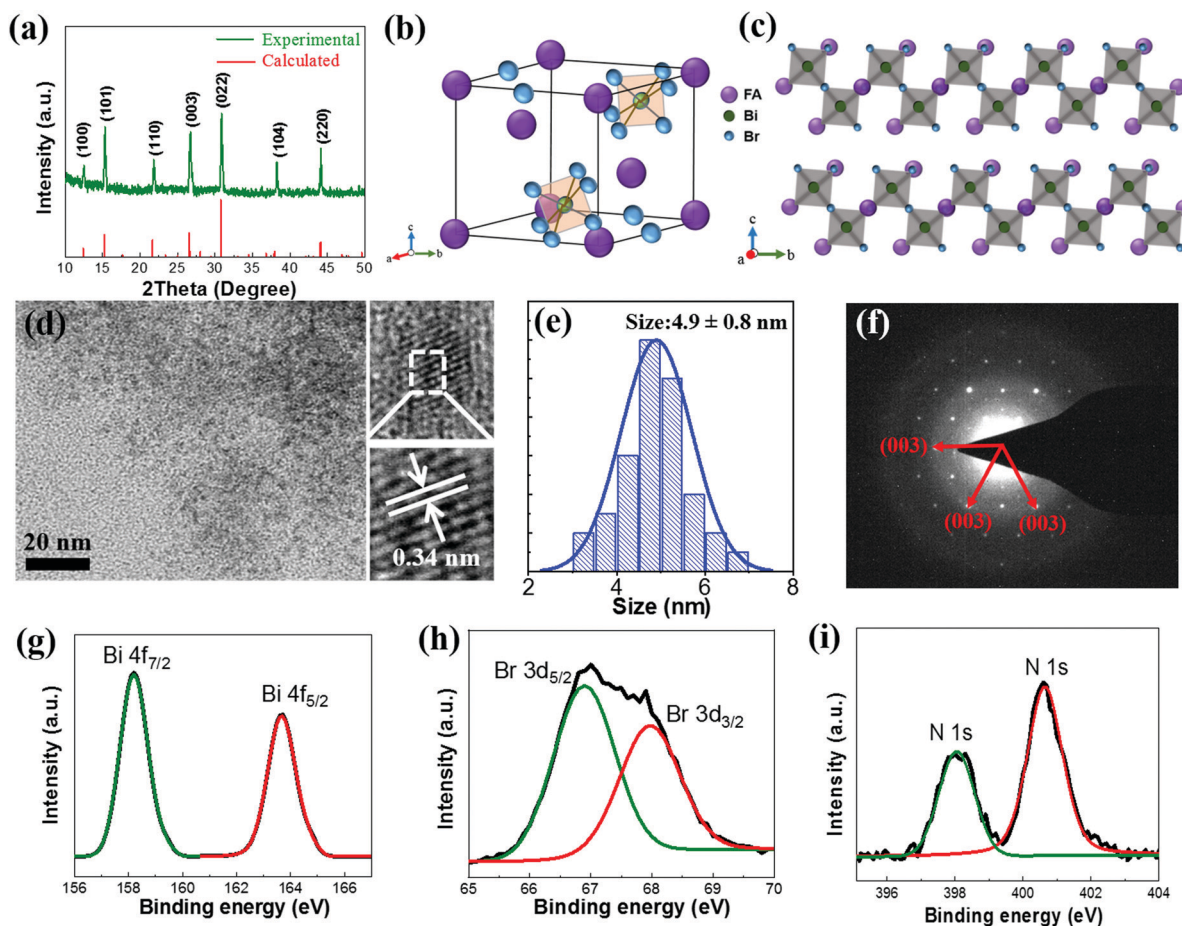
Fig. 1 (a) XRD pattern of the as-prepared $FA_3Bi_2Br_9$ powders. Diagram of the (b) $FA_3Bi_2Br_9$ unit cell and (c) crystal structure. (d) TEM (left) and HRTEM (right) images of $FA_3Bi_2Br_9$ QDs. (e) Size distribution histogram of $FA_3Bi_2Br_9$ QDs. (f) The SAED of $FA_3Bi_2Br_9$ QDs. High-resolution XPS spectra and peak fitting of (g) Bi 4f, (h) Br 3d and (i) N 1s for $FA_3Bi_2Br_9$ QDs.

in lighting applications. The excitation peak of the $FA_3Bi_2Br_9$ QDs is located at 350 nm, as demonstrated by the excitation wavelength (Fig. S4, ESI†).

To obtain the mixed halide perovskite QDs, we have synthesized $FA_3Bi_2X_9$ (X = Cl, Br, and I) QDs by controlling anion exchange reactions. Diffuse reflectance UV-Vis spectroscopy was performed and the corresponding Tauc plots are depicted in the inset of Fig. 2c. The bandgaps increase once Br atoms were partially replaced by Cl or decreased by I, leading to composition-dependent photoluminescence (the emission PL peak shifts from 399 to 526 nm, Fig. 2b). Therefore, the bandgap of $FA_3Bi_2X_9$ varied from 2.46 to 3.09 eV with a change in X from Cl to I (Fig. 2c). Bandgap values were obtained by assuming that these mixed $FA_3Bi_2X_9$ perovskites are direct bandgap materials, which could be verified *via* subsequent DFT calculations. The change in the color of samples was found to be in agreement with the trend in bandgap shift, as shown in Fig. S5 (ESI†). Furthermore, the comparison of PLQY, emission peak and FWHM between $FA_3Bi_2Br_9$ QDs and the as-prepared $FA_3Bi_2Cl_9$ and $FA_3Bi_2I_9$ is summarized in Table S2 (ESI†).

Among these QDs, $FA_3Bi_2Br_9$ shows an experimental bandgap of 2.87 eV, which is consistent with the calculated value (a direct bandgap of 2.84 eV at the Γ-point, Fig. 3a). For the

projected density of states (PDOS) as presented in Fig. 3b, the valence band maximum (VBM) of $FA_3Bi_2Br_9$ is composed of both Br-4p and Bi-6s, and the conduction band minimum (CBM) is mostly contributed by the Bi-6p (Fig. S6, ESI†), in accordance with the properties of the direct bandgap Pb-based perovskites (the VBM is primarily composed of halide-p orbital, while the CBM has mostly Pb-p orbital character).[30,31] This indicates that the absorption continuum is due to the interband electronic transitions with the main contributions coming from $Bi^{3+}(6s)Br^-(4p) \rightarrow Bi^{3+}(6p)$ around the Γ point. Our DFT results also suggest that the lone pair *s* electrons (Bi-6s) are one of the prerequisites for achieving the excellent optical properties of the $FA_3Bi_2X_9$ system.[32] (Note that the Bi-6s shows a low occupation in the PDOS results because of the low electron ratio of Bi/Br, but it contributes greatly to the optical properties of the perovskite.)

We further conducted the time-resolved PL measurements to reveal the exciton recombination dynamics of the $FA_3Bi_2Br_9$ QDs. Fig. 3c shows the PL decay of the $FA_3Bi_2Br_9$ QDs under different light intensities (2.4, 7.7, 24 μW). All the PL decay curves show monoexponential decay behavior, and by fitting the PL decay curves with the monoexponential model, the corresponding PL lifetimes of 3.54, 3.51 and 3.45 ns are obtained, respectively. Upon the unchanged monoexponential PL lifetime behavior,
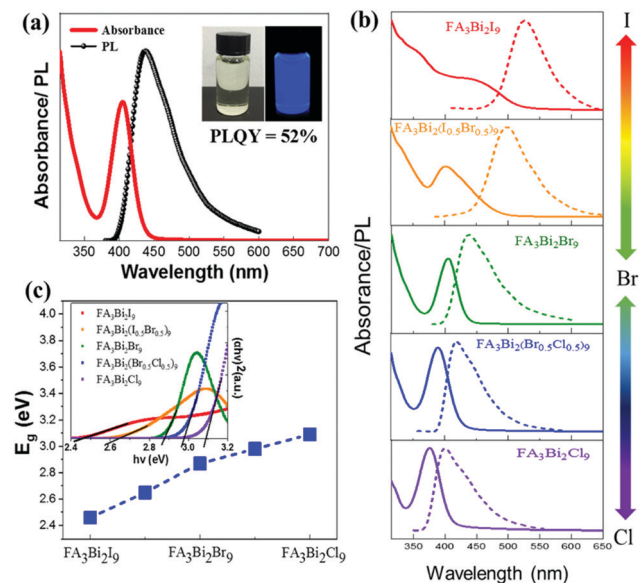
Fig. 2 (a) Normalized PL and UV-Vis absorption spectra of $FA_3Bi_2Br_9$ QDs. Insets: Optical photographs of the colloidal $FA_3Bi_2Br_9$ solution under visible light and UV light. (b) Controllable PL and absorption spectra of $FA_3Bi_2X_9$ (X = Cl, Br, and I) QDs with different compositions. (c) Calculated bandgap results of $FA_3Bi_2X_9$. The inset: Normalized Tauc plots of the typical absorption spectra of $FA_3Bi_2X_9$ QDs for evaluating the bandgap values, assuming a direct bandgap feature.

the $FA_3Bi_2Br_9$ QDs are believed to have an extremely low defect density due to the surface-passivation, which favors radiative recombination and leads to a high PLQY. Generally, the obtained short-lived lifetime can be attributed to exciton recombination, and the monoexponential fitting results give reasonably good agreement with the high PLQY of 52% of the $FA_3Bi_2Br_9$ QDs.

To further explore the mechanism of photoluminescence decay in $FA_3Bi_2Br_9$ QDs, the temperature-dependent PL measurements were performed. Taking into account the activation of nonradiative recombination centers in $FA_3Bi_2Br_9$ perovskite, we chose the temperature range of 208–298 K to analyze the temperature-dependent PL spectra.[26] As presented in Fig. S7a (ESI†), the PL intensity exhibited obvious increase with decreasing temperature. Fig. S7b (ESI†) shows the integrated PL intensity *versus* temperature, and the curve can be fitted using the eqn (1)
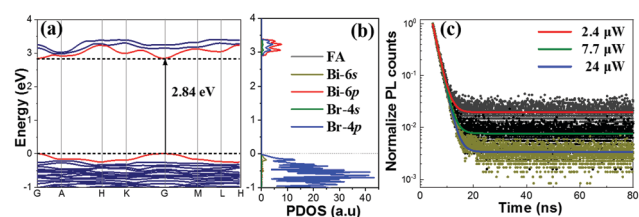
$$I(T) = \frac{I_0}{1 + A e^{-E_b/Tk_B}} \tag{1}$$

where I_0 is the intensity at 0 K, k_B is the Boltzmann constant and E_b is exciton binding energy. From the fitting analysis, the exciton binding energy of $FA_3Bi_2Br_9$ is estimated to be 274.6 meV; such large E_b can be attributed to the strong quantum confinement effect of QDs, which ensures the generation of excitons at room-temperature and promotes their efficient recombination, and hence the QDs are prone to exhibit higher PL intensity. Besides, here the contribution of toluene is indispensable for their binding enhancement. In principle, a lower surrounding dielectric constant usually leads to a higher E_b due to the dielectric confinement effect.[33] In this system, toluene with low-dielectric-constant acts as the solvent of the colloidal $FA_3Bi_2Br_9$ QDs, resulting in lower surrounding dielectric constant, and thereby increasing the E_b of $FA_3Bi_2Br_9$ QDs.

The air stability of the $FA_3Bi_2Br_9$ QDs was investigated by measuring the PL intensity evolution under ambient conditions. As illustrated in Fig. 4a, after storage in the air for 30 days, we can still achieve 75% PL intensity of the QDs without any encapsulation as compared to that of the fresh sample (the insets in Fig. 4a show the photographs of QDs under UV irradiation). Based on the good air stability performance, we built an encapsulation of QDs by simply mixing the QDs with a common polymer polystyrene (PS). This one-pot encapsulation is well suitable for our $FA_3Bi_2Br_9$ QDs because of their superior flexibility. The $FA_3Bi_2Br_9$ QDs/PS composite was exactly demonstrated to have an excellent flexibility, as presented in the inset of Fig. 4b. Next, PLQY evolution measurements were conducted for the QDs and QDs/PS composites (Fig. 4b). Unexpectedly, in the first few days of storage, the PLQY undergoes a little degree of improvement. Such PLQY enhancement is probably due to the "photoactivation" phenomenon, benefitting from the smoothing of $FA_3Bi_2Br_9$ QDs and the removal of dangling bonds or some surface defects.[26] During the further storage, the PLQY of the $FA_3Bi_2Br_9$ QDs/PS showed a gradual decrement due to the surface defects induced by oxygen exposure, this phenomenon was similar to that of Pb-based perovskites. After 30 days of storage, the QDs/PS composite can still keep 95% of the PLQY as compared to the 73% of the PLQY of QDs without encapsulation, implying the efficient encapsulated protection from the polymer PS. Furthermore, we investigated the stability of $FA_3Bi_2Br_9$ QDs in ethanol. Interestingly, by adding 1 mL of ethanol into 1 mL of the as-prepared $FA_3Bi_2Br_9$ QD solution, the PL intensity only shows

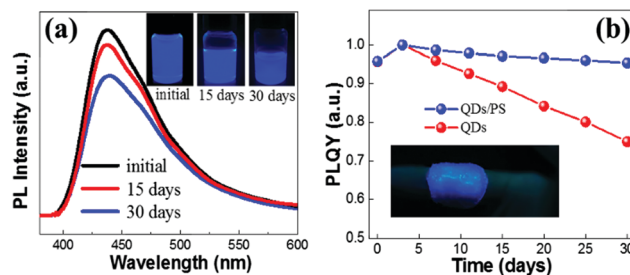Fig. 3 (a) The electronic band structures and (b) projected density of states (PDOS) of $FA_3Bi_2Br_9$ calculated at the GGA/PBE level of theory. (c) The time-resolved PL of $FA_3Bi_2Br_9$ QDs under different excitation intensities.

Fig. 4 (a) The PL intensities of $FA_3Bi_2Br_9$ QDs at initial, 15 days and 30 days, insets: the corresponding photographs of $FA_3Bi_2Br_9$ solutions at each time under UV irradiation. (b) Comparison of the air-stability for $FA_3Bi_2Br_9$ QDs and $FA_3Bi_2Br_9$ QDs/PS composites under ambient conditions. The inset shows the $FA_3Bi_2Br_9$ QDs/PS composite deposited on the finger.
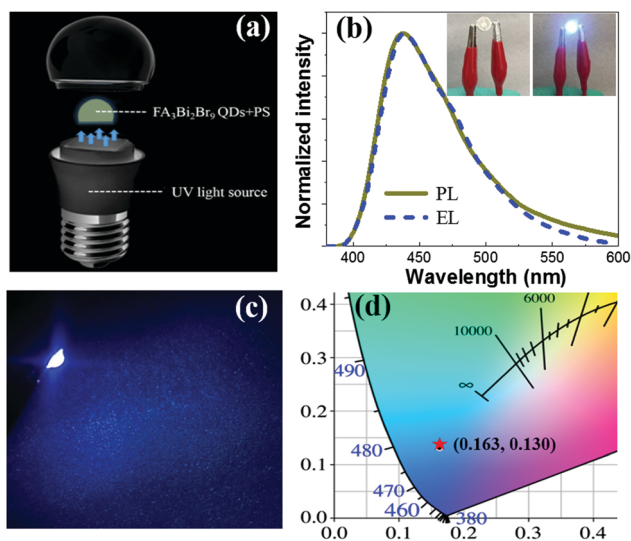
Fig. 5 (a) Diagram of the LED device combining UV light chips with QDs/PS composites. (b) EL and PL spectra of the LED and the $FA_3Bi_2Br_9$ QDs, respectively. The insets show the device in closed and open states. (c) Fluorescence image of the LED. (d) CIE coordinates of $FA_3Bi_2Br_9$ QDs in CIE 1931 space.

a slight decrease (Fig. S8, ESI†), which demonstrates the much more stable performance than $FAPbBr_3$ perovskite in terms of the endurance for ethanol.

To date, there are few research studies about light-emitting diodes (LEDs) based on Pb-free halide perovskite QDs. The capability of fine emission tuning in the highly desirable wavelength of 437 nm, along with high PLQY, and good air stability, make the $FA_3Bi_2Br_9$ QDs suitable for light-emitting device applications. Blue LEDs were assembled through combining UV light chips (rongcheng mic-electronics Co. Ltd, ShenZhen) and $FA_3Bi_2Br_9$ QDs/PS composite (Fig. 5a). Separated high-energy UV light sources for photoexcitation were applied to emit blue emission from the $FA_3Bi_2Br_9$ QDs. As a result, the as-fabricated blue LED well maintained the electroluminescence (EL) emissions at 437 nm (Fig. 5b), which barely shifts in comparison to the PL spectrum. This means that the $FA_3Bi_2Br_9$ QDs keep their original electronic structure and properties under ambient voltage. Furthermore, the device well maintained the EL emissions in a wide range of operating currents from 20 to 100 mA (Fig. S9, ESI†). A maximum EQE of 3.05% was obtained, as shown in Fig. S10, ESI.† The insets of Fig. 5b present the photographs of the devices in closed and open states. Notably, bright blue color emitted from the underlying UV chips through photoluminescence by the $FA_3Bi_2Br_9$ QDs are shown in Fig. 5c, indicating superior lighting effects for the $FA_3Bi_2Br_9$ QDs (Table S3, ESI†). The CIE 1931 color coordinate of (0.163, 0.130) corresponding to the blue LED is shown in Fig. 5d. The satisfactory EL performance of $FA_3Bi_2Br_9$ QDs and their good air-stability were expected to hold great potential in wide applications including lighting, lasing and so on.

Conclusions

In summary, an appealing solution-processed method was developed for the synthesis of well-defined Pb-free $FA_3Bi_2Br_9$ QDs,

and bright blue emission (437 nm), and high absolute PLQY (52%) were achieved at room temperature. The high PLQY value represents the top level among Pb-free perovskite QDs in the same wavelength region. By varying different precursor solutions, the fine-tuned $FA_3Bi_2X_9$ QDs composition was obtained with the emission peak ranging from 399 to 526 nm. The $FA_3Bi_2Br_9$ was proposed to have a direct bandgap of 2.84 eV by DFT, showing good agreement with the experimental data. The extremely low defect density and high E_b of the QDs, were supported to achieve ultrahigh PLQY. Furthermore, the $FA_3Bi_2Br_9$ QDs exhibit a good air stability and excellent ethanol stability. To fulfill the practical applications, an LED with bright blue color was fabricated based on these QDs. This work will open a new avenue to obtain high-quality blue color perovskite QDs, and provide a good candidate for Pb-free perovskite LED applications.

Conflicts of interest

There are no conflicts to declare.

Acknowledgements

References

1 C. Liu, H. Peng, K. Wang, C. Wei, Z. Wang and X. Gong, *Nano Energy*, 2016, **30**, 27–35.

2 H. Wei, Y. Fang, Y. Yuan, L. Shen and J. Huang, *Adv. Mater.*, 2015, **27**, 4975–4981.

3 Y. Wang, K. Lu, L. Han, Z. Liu, G. Shi, H. Fang, S. Chen, T. Wu, F. Yang, M. Gu, S. Zhou, X. Ling, X. Tang, J. Zheng, M. A. Loi and W. Ma, *Adv. Mater.*, 2018, **30**, 1704871.

4 H. Sun, Z. Yang, M. Wei, W. Sun, X. Li, S. Ye, Y. Zhao, H. Tan, E. L. Kynaston, T. B. Schon, H. Yan, Z. H. Lu, G. A. Ozin, E. H. Sargent and D. S. Seferos, *Adv. Mater.*, 2017, **29**, 1701153.

5 C. Xie, P. You, Z. Liu, L. Li and F. Yan, *Light: Sci. Appl.*, 2017, **6**, 17023.

6 Y. Shen, C. Wei, L. Ma, S. Wang, X. Wang, X. Xu and H. Zeng, *J. Mater. Chem. C*, 2018, **6**, 12164–12169.

7 X. Li, F. Cao, D. Yu, J. Chen, Z. Sun, Y. Shen, Y. Zhu, L. Wang, Y. Wei, Y. Wu and H. Zeng, *Small*, 2017, **13**, 1603996.

8 Y. Wang and H. Sun, *Small Methods*, 2018, **2**, 1700252.

9 M. I. Saidaminov, A. L. Abdelhady, B. Murali, E. Alarousu, V. M. Burlakov, W. Peng, I. Dursun, L. Wang, Y. He, G. Maculan, A. Goriely, T. Wu, O. F. Mohammed and O. M. Bakr, *Nat. Commun.*, 2015, **6**, 7586.

10 L. Lv, Y. Xu, H. Fang, W. Luo, F. Xu, L. Liu, B. Wang, X. Zhang, D. Yang, W. Hu and A. Dong, *Nanoscale*, 2016, **8**, 13589–13596.

11 Q. Shan, J. Song, Y. Zou, J. Li, L. Xu, J. Xue, Y. Dong, B. Han, J. Chen and H. Zeng, *Small*, 2017, **13**, 1701770.

12 J. Liang, C. Wang, P. Zhao, Z. Lu, Y. Ma, Z. Xu, Y. Wang, H. Zhu, Y. Hu, G. Zhu, L. Ma, T. Chen, Z. Tie, J. Liu and Z. Jin, *Nanoscale*, 2017, **9**, 11841–11845.

13 N. Yantara, S. Bhaumik, F. Yan, D. Sabba, H. A. Dewi, N. Mathews, P. P. Boix, H. V. Demir and S. Mhaisalkar, *J. Phys. Chem. Lett.*, 2015, **6**, 4360–4364.

14 F. Jiang, D. Yang, Y. Jiang, T. Liu, X. Zhao, Y. Ming, B. Luo, F. Qin, J. Fan, H. Han, L. Zhang and Y. Zhou, *J. Am. Chem. Soc.*, 2018, **3**, 1019–1027.

15 F. Giustino and H. J. Snaith, *ACS Energy Lett.*, 2016, **1**, 1233–1240.

16 J. Sun, J. Yang, J. I. Lee, J. H. Cho and M. S. Kang, *J. Phys. Chem. Lett.*, 2018, **9**, 1573–1583.

17 A. Abate, *Joule*, 2017, **1**, 659–664.

18 T. C. Jellicoe, J. M. Richter, H. F. J. Glass, M. Tabachnyk, R. Brady, S. E. Dutton, A. Rao, R. H. Friend, D. Credgington, N. C. Greenham and M. L. Boehm, *J. Am. Chem. Soc.*, 2016, **138**, 2941–2944.

19 X. Qiu, Y. Jiang, H. Zhang, Z. Qiu, S. Yuan, P. Wang and B. Cao, *Phys. Status Solidi RRL*, 2016, **10**, 587–591.

20 A. Wang, X. Yan, M. Zhang, S. Sun, M. Yang, W. Shen, X. Pan, P. Wang and Z. Deng, *Chem. Mater.*, 2016, **28**, 8132–8140.

21 X. F. Qiu, B. Q. Cao, S. Yuan, X. F. Chen, Z. W. Qiu, Y. A. Jiang, Q. Ye, H. Q. Wang, H. B. Zeng, J. Liu and M. G. Kanatzidis, *Sol. Energy Mater. Sol. Cells*, 2017, **159**, 227–234.

22 S. Gupta, T. Bendikov, G. Hodes and D. Cahen, *ACS Energy Lett.*, 2016, **1**, 1028–1033.

23 D. Parobek, B. J. Roman, Y. Dong, H. Jin, E. Lee, M. Sheldon and D. H. Son, *Nano Lett.*, 2016, **16**, 7376–7380.

24 W. J. Mir, M. Jagadeeswararao, S. Das and A. Nag, *ACS Energy Lett.*, 2017, **2**, 537–543.

25 M. Y. Leng, Z. W. Chen, Y. Yang, Z. Li, K. Zeng, K. H. Li, G. D. Niu, Y. S. He, Q. C. Zhou and J. Tang, *Angew. Chem., Int. Ed.*, 2016, **55**, 15012–15016.

26 M. Leng, Y. Yang, K. Zeng, Z. Chen, Z. Tan, S. Li, J. Li, B. Xu, D. Li, M. P. Hautzinger, Y. Fu, T. Zhai, L. Xu, G. Niu, S. Jin and J. Tang, *Adv. Funct. Mater.*, 2018, **28**, 1704446.

27 J. Zhang, Y. Yang, H. Deng, U. Farooq, X. K. Yang, J. Khan, J. Tang and H. S. Song, *ACS Nano*, 2017, **11**, 9294–9302.

28 B. Yang, J. Chen, F. Hong, X. Mao, K. Zheng, S. Yang, Y. Li, T. Pullerits, W. Deng and K. Han, *Angew. Chem., Int. Ed.*, 2017, **56**, 12471–12475.

29 D. Zhang, S. W. Eaton, Y. Yu, L. Dou and P. Yang, *J. Am. Chem. Soc.*, 2015, **137**, 9230–9233.

30 Q. Lin, A. Armin, R. C. R. Nagiri, P. L. Burn and P. Meredith, *Nat. Photonics*, 2014, **9**, 106–112.

31 M. D. Smith and H. I. Karunadasa, *Acc. Chem. Res.*, 2018, **51**, 619–627.

32 A. Walsh, D. J. Payne, R. G. Egdell and G. W. Watson, *Chem. Soc. Rev.*, 2011, **40**, 4455–4463.

33 S. Kumar, J. Jagielski, N. Kallikounis, Y. H. Kim, C. Wolf, F. Jenny, T. Tian, C. J. Hofer, Y. C. Chiu, W. J. Stark, T. W. Lee and C. J. Shih, *Nano Lett.*, 2017, **17**, 5277–5284.